Ionomer Thin Films in PEM Fuel Cells

Ahmet Kusoglu
Energy Conversion Group, Energy Technologies
Area, Lawrence Berkeley National Laboratory,
Berkeley, CA, USA

Article Outline

Glossary
Definition of the Subject
Introduction: Ionomers in Fuel Cells
Ionomer Thin Films
Summary and Remarks
Future Directions
Bibliography

Glossary

Ionomer membranes ionomers that are cast, fabricated, and used as a bulk material with a thickness on the order of micrometers. Most PEMs in fuel cells are 10 to 200 μm thick but are expected to be thinner and robust for sustainable cell performance.

Ionomer thin films ionomers that are cast on, and interact with, a support material (substrate) thereby forming a thin film with a thickness on the order of nanometers. In fuel cell catalyst layers (CLs), ionomers exist as nanometer-thick electrolyte film responsible for transporting ions and reactants to catalyst sites, where electrochemical reactions occur.

Ionomer an ion-containing polymer chemically composed of charged (ionic) groups tethered to an electrically neutral polymer backbone. The fixed ionic groups are neutralized by the mobile counterions of opposite charge, which act as charge carriers, thereby giving the ionomer its inherent ion-conductive functionality. Ionomers are commonly used as the PEM in fuel cells.

PFSA (perfluorosulfonic acid) a fluorocarbon-based sulfonated ionomer, which is a random copolymer of a polytetrafluoroethylene (PTFE) backbone and a randomly tethered polysulfonyl fluoride vinyl ether side chain terminated by the polar sulfonic acid ionic group, SO_3^-, that is associated with a specific counterion, most commonly a proton (e.g., $SO_3^- + H^+ \rightarrow SO_3H$). Nafion® is a commercially available PFSA developed by DuPont in the 1960s, which has since been adopted as a benchmark PEM in fuel cells.

Proton exchange membrane (PEM) a polymeric membrane that separates the electrodes in an electrochemical device, such as a fuel cell, and conducts protons between the electrodes while separating their reactant gases.

Definition of the Subject

In polymer-electrolyte fuel cells (PEFCs), ionomers play a key role not only as a proton exchange membrane (PEM) but also as nanometer-thick electrolyte "thin films" within porous catalyst layer (CL) structures, where they bind and cover the catalytic particles and provide transport pathways for the ions and reactant species. An ionomer's properties and functionality are governed by its hydration-dependent nanostructure, which separates into hydrophilic transport pathways and hydrophobic polymer matrix. As the ionomer is confined to nanometer thicknesses in the CLs, its intrinsic nano-morphology and resulting transport properties deviate from bulk membrane behavior. These deviations in properties manifest themselves as additional resistance to transport of active species that are key for driving the desired electrochemical reactions. Thus, some of the performance losses observed in the cell are rooted in the catalyst ionomer and its

local environment and interactions therein. In thin-film form, the ionomer forms dynamic interfaces with the air and substrate, which impose stronger impact on ionomer's structure/functionality. This interplay between the confinement and dynamic interactions controls the catalyst ionomer's properties, which affects the local transport resistances in CLs, and ultimately PEFC performance.

Introduction: Ionomers in Fuel Cells

Perfluorosulfonic acid (PFSA) ionomers are ion-conducting polymers commonly used as the solid electrolyte/separator in electrochemical energy conversion and storage devices where they provide multiple functionalities such as ion conductivity, gas separation, and solvent transport. Similarly, in polymer electrolyte fuel cells (PEFCs), PFSA ionomers have been widely studied and used as the PEM with a thickness on the order of micrometers (10 to 200 μm); yet, increasingly important, but less explored, is the role of ionomers as thin films and the interfaces they form within the heterogeneous catalyst layer structures, where electrochemical reactions occur (see Fig. 1). In particular, the latter phenomenon of confinement could have important implications for the mass-transport limitations in catalyst layers and PEFC performance, which are strongly related to the transport resistances occurring within the ionomer thin film and at its interfaces.

In a catalyst layer (CL), the ionomer functions as nanometer-thick electrolyte film binding the catalyst particles together and facilitating proton transport through the layer and gas and water transport to and from the catalytic sites. A CL is a heterogeneous porous structure to increase electrocatalytically active surface area, where the ionomer thin film provides proton transport pathways to platinum particles, the carbon particles provide electron conduction, and the pores enable gas/liquid transport (see Fig. 1). Thus, while the ionomer's proton transport functionality persists throughout the membrane-electrode assembly, i.e., from PEM to CLs, and is critical to the cell performance, the ionomer's gas transport

functionality differs significantly within the cell. Ionomer as a PEM functions not only as a solid electrolyte but also as a (gas) separator requiring low O_2 permeability, whereas the ionomer in the cathode CL must allow ingress of O_2 molecules from pores to the catalytic Pt sites, where they meet electrons (transferred through carbon) and reduce O_2 to water (Fig. 1). Hence, an ionomer's gas transport functionality exhibits a striking contrast between PEM (gas impermeable) and CL (gas permeable), understanding and optimization of which is critical for cell design and performance [1–15].

The current state of CL diagnostics data suggests that the local resistance arising from the ionomer/Pt interfaces in CL decreases with increasing Pt loading, [1, 2, 6–15] exemplifying how the performance and cost could be intertwined [1, 7] (also see the chapter ▶ "Proton-Exchange Membrane Fuel Cells with Low-Pt Content" by A. Kongkanand). The overall reaction rate in the cathode CL is slow due to the formation of water, the four-electron process of O_2 reduction, and the use of air as the O_2 carrier, thereby resulting in dramatic performance losses. Because the oxygen reduction reactions (ORR) take place at the ionomer/Pt interface, ionomer interactions are believed to play a key role in controlling the transport resistance in CLs. The contributions to the O_2 transport resistance in CLs illustrated in Fig. 1: (i) O_2 transport at the ionomer/air interface, (ii) O_2 permeation and diffusion through the ionomer film, and (iii) O_2 permeation at the ionomer/Pt interface. Despite distinct physicochemical natures of each mechanism, they are all related to the behavior of ionomer moieties and their interaction with the water and gas molecules, as well as the substrate composition. Given the unequivocal goal of reducing the Pt loading (and cost), these transport phenomena create an intriguing performance-cost trade-off, which is considered one of the most critical challenges that must be addressed in PEM fuel cells to make them a competitive technology [1, 2, 7].

Ionomers exist in CLs with a distribution of thicknesses ranging from 7 to 15 nm [2, 4, 16], which could be influenced by several design parameters, such as the ratio of carbon to ionomer (C/I), porosity, Pt loading, as well as CL

Polymer-Electrolyte Fuel Cells (PEFCs): Role of Ionomers
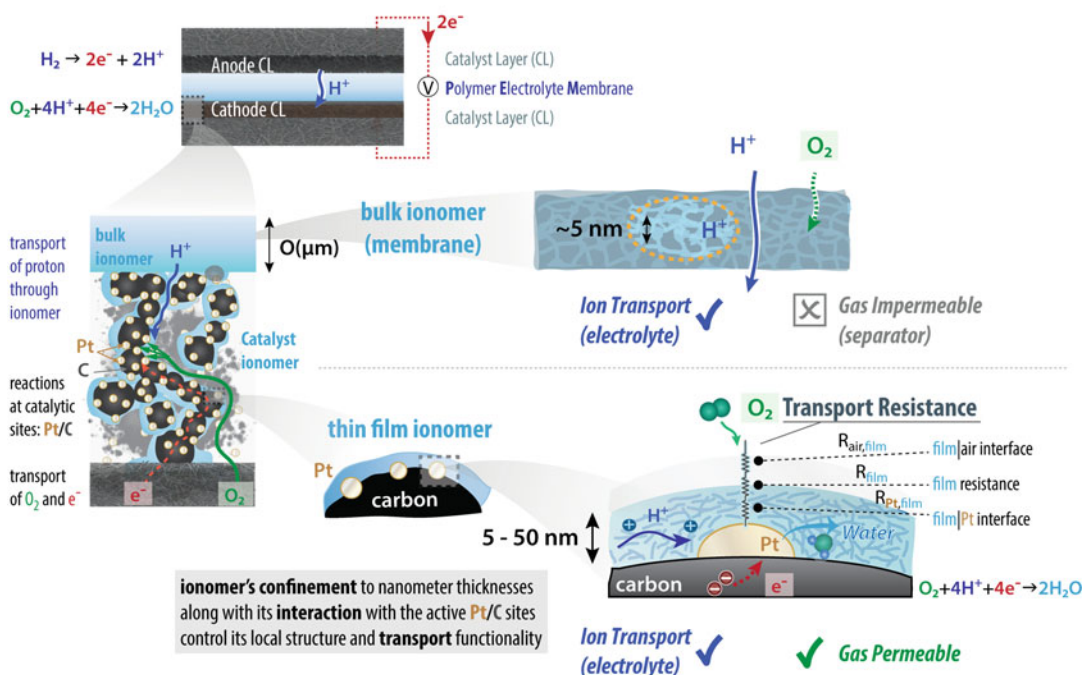
Ionomer Thin Films in PEM Fuel Cells, Fig. 1 Role of ionomers in PEM fuel cells as an ion-conducting polymer electrolyte membrane (PEM) and catalyst ionomer in the electrodes

fabrication method. Thus, the ionomer thickness (distribution) is likely to change with the ionomer fraction in the CL, which affects the surface area and mass activity of CL therein [10–12, 17]. Similarly, water uptake behavior of catalyst ionomer changes with C/I ratio [3, 9, 10, 17, 18], type of carbon support [6], Pt loading [18], as well as pretreatment [18]. The nature of Pt surface also impacts the water uptake; catalyst ionomer under reducing environment absorbs less water due to the removal of oxide layer, the presence of which creates a oxide-rich PtO layer that is more polar and hydrophilic [19]. The complex structure of CL, wherein the ionomer film formation and properties are controlled by a multitude of parameters listed in Table 1, has driven the need for developing model systems for ionomers. Thin-film ionomers serve this purpose with an idealized representation of CL ionomers (Table 1). Thin films are prepared by casting a diluted ionomer dispersion onto a uniform, homogenous support substrate followed by thermal treatments and other post-processing treatments. The most commonly used technique is spin casting, where the ionomer dispersion with a dilute concentration of solid is cast on a substrate spinning at a controlled rate, followed by other methods such as self-assembly or drop casting on a substrate. Due to the distinct nature of these processes, casting methods and conditions influence the structure/ property relationship of the ionomer film, as do the substrate and the dispersion solvents, because of their interaction with the ionomer moieties [20]. As the casting and dispersion solvent also affects both the CL structure and PEM [2, 21–23], fundamental investigation of such processing effects in ionomer thin films could be beneficial for developing material solutions for improved cell performance. The key aspects and parameter space of thin films and their diagnostics are shown in Table 1 and Fig. 2, respectively. Even though thin films underestimate the heterogeneity and binary interactions in CL ionomers, they nonetheless provide a mean to isolate and study some of

Ionomer Thin Films in PEM Fuel Cells, Table 1 Comparison of ionomers in fuel cell catalyst layers and ionomer thin films as model systems

	Catalyst layer ionomer	Ionomer thin film
Use/function	PEM fuel cell electrode	Thin-film model system
Film formation	Through casting and processing of catalyst inks containing ionomer dispersion	Casting from a dispersion onto a support substrate (e.g., spin casting)
Design and structure	Heterogeneous porous structure where ionomer covers particles on nonplanar surfaces	Homogeneous, macroscopically uniform structure on a planar substrate surface
Design and material parameters	Carbon and Pt type and fraction, ionomer content, CL thickness and porosity, coating method and conditions, ionomer chemistry, casting solvent	Substrate, ionomer chemistry, casting solvent (dispersion), casting method and conditions
Thickness	Varies with spatial distribution, C:I ratio, and Pt loading	Constant film thickness controlled during casting
Interactions	Dynamic interactions with catalytic particles including carbon and platinum	Interactions with the substrate
Operational parameters	RH, T, potential and time	RH, T, potential and time
Conditioning	Cell conditioning and break-in protocols affecting ionomer	Thermal and solvent annealing of films after casting

these effects in an effort to identify the governing factors and phenomena. Thus, ionomer thin films allow characterizing an ionomer's morphology, measuring its swelling and transport properties, and probing its interactions with the substrate, under controlled environments. Such investigations, in most cases, require techniques specifically suited for thin films that are distinct from those used to characterize bulk membranes (see Fig. 2).

The challenges common to these techniques include significantly less volume occupied by the thin films and the influence of the substrate composition on the ionomer, which requires a careful examination and analysis of the measured properties. Nevertheless, most surface characterization techniques are applicable to both bulk and thin-film form of the ionomer, and any observed difference between the two could also be used to study the interfacial effects and their domain of influence through the thickness of the ionomer.
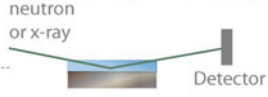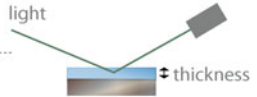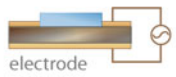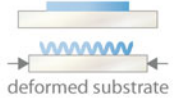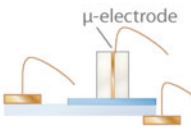
Ionomer Thin Films

A PFSA ionomer is comprised of hydrophilic domains of 3 to 6 nm that are interconnected and form a phase-separated network at longer length scales (100s of nm), which ultimately controls its macroscopic properties. When the thickness of ionomer is reduced to 100 nm or below, its constituent chains and moieties are confined to volumes comparable to its characteristic domain size, thereby losing their ability to form a bulk-like morphology. Such nanoconfinement of an ionomer also amplifies the overall impact of the substrate interactions on the thin film, which, in turn, could further restrict the ionomer moieties' mobility and cause additional nanostructural changes, as highlighted in Fig. 3.

Even though confinement effects in polymer thin films have long been of interest [47–52], their application to charge-containing ionomer thin films used in PEM fuel cells has garnered interest only recently [6, 9, 20, 25, 27, 30, 32, 33, 36, 37, 53–57], due primarily to the need for understanding the ionomer behavior in PEFC electrodes [1, 2, 7–9, 13, 14].

Confinement effects are strongly intertwined with the surface morphology and properties of bulk ionomers (i.e., PEM), where the ionomer forms a thin layer of interfacial "skin" that behaves differently from the ionomer in the

Ionomer Chararacterization and Diagnostics

Bulk membrane
Thickness: 10 to 200 µm

Thin Film (on a substrate*)
Thickness: 10 to 500 nm

Morphology
X-ray scattering (XS)   Grazing-incidence XS
Neutron scattering   Neutron reflectivity

Swelling
Dimensional change   Spectroscopic Ellipsometry

Water Uptake
Gravimetric (weight)   Quartz-crystal microbalance

Ion Transport (Conductivity)
Electrochemical cell   Impedance measurement
or impedance setup   of film on a inter-digitated
(e.g., four-probe in-plane or array (substrate)
thickness direction)

Mechanical Response
Stress-Strain testing   Buckling on a support
DMA, TMA   Cantilever beam bending

Gas Transport
permeation   microelectrode setup

Techniques Probing Surface
AFM, contact angle, FTIR/ATR, XPS

* ionomer film's property is measured on a support substrate,
and affected by the substrate and its interaction with the film

Ionomer Thin Films in PEM Fuel Cells, Fig. 2 Comparison of characterization and diagnostic techniques commonly used for bulk ionomers and thin-film ionomers, which are conceptualized with simplified schematics for selected techniques. Additional information on technique can be obtained in the references [20, 24] and [25–29] for morphology [20, 27, 30–33], for swelling and uptake [34–37], for conductivity [26, 38], for mechanical properties [8, 13, 15, 39], for microelectrode [40–46], and for spectroscopy techniques

internal regions (see Fig. 3). This surface layer in bulk ionomer could influence the membrane's transport properties by controlling the mass transport of species through its interface [58–61], although the membrane's overall behavior is still controlled by its internal regions, which constitute the majority of the material's volume (Fig. 3). As the thickness of the ionomer is reduced to sub-micrometer values, however, the interfacial effects are more pronounced. In the thin-film motif, in contrast with the ionomer's open surface that creates an interfacial layer, its other surface interacts with the solid substrate. Therefore, an ionomer thin film's behavior is influenced by these two key interactions, both of which propagate through the ionomer thin film, but in the opposite directions, and perhaps with different strengths (Fig. 3). Once the film thickness reaches below 100 nm, a strong interplay between the confinement and substrate interactions controls the ionomer's nanostructure and properties. As the film thickness approaches 10s of nanometers,
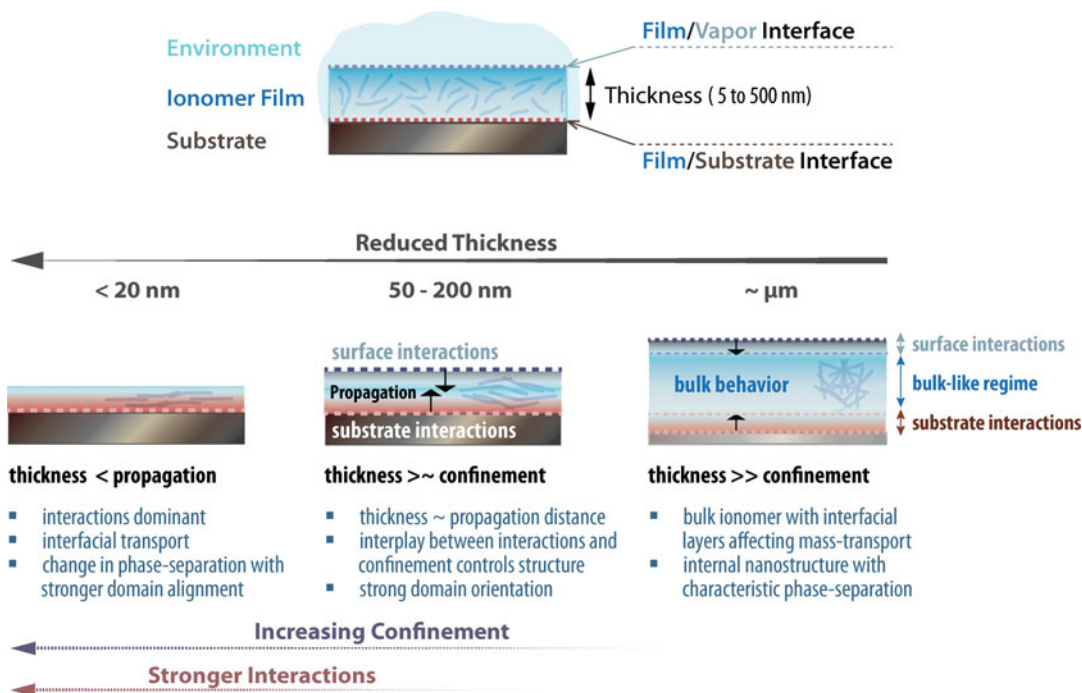
Ionomer Thin Films in PEM Fuel Cells, Fig. 3 Impact of thickness on properties of PFSA ionomers from bulk membrane to the confined thin films highlighting the interplay between the surface/substrate interactions and confinement controlling the morphology of the ionomer

i.e., comparable to CL ionomers, the impact of substrate interactions becomes dominant. Thus, in the thin-film regime, ionomer properties deviate significantly compared to its bulk form (i.e., PEM), and the magnitude of these deviations depends on the substrate and the environment (Fig. 4).

Recent years have witnessed a significant effort dedicated toward understanding PFSA thin films, which exhibit reduced transport properties compared to those of bulk films due to abovementioned confinement effects [1, 20, 27, 32, 33, 36, 37, 53–57, 62–65]. Compared to bulk membrane, Nafion® films of ~100 nm or thinner have been shown to exhibit reduced swelling [20, 27, 33, 66, 67], water uptake amounts and rates [20, 24, 27, 32, 33, 36, 54, 56, 57, 64, 65, 68], reduced ionic conductivity and increased activation energy [5, 34, 36, 37, 53, 56, 64, 69, 70], lower rate of water diffusion [27, 54, 65, 68, 71, 72], lower intrinsic permeation [73], lower contact angle [45, 67, 70], higher fraction of hydrophilic surface area [70], higher modulus

[26, 38], and lower oxygen permeability [8, 13, 39]. Figure 4 highlights the relative changes in selected properties of Nafion thin films compared to their values for thicker Nafion. Upon confinement to nanometer thicknesses, transport properties for proton and oxygen in Nafion decrease up to more than 50%, while their activation barrier increases indicating an overall significant increase in the transport resistance. The fact that the magnitude of these changes depends on the measured property and the environmental conditions reflects the complex nature of ionomer film's structure and interactions with the substrate (on which the properties are measured).

These studies demonstrate trends reflecting the confinement effects below 100 nm, and significant shifts in the values along with stronger effect of substrates as the film thickness reduces below 50 nm and approaches 10 nm [20, 24, 27, 31–33, 36, 37, 40, 45, 53–56, 63–67, 70]. Confinement, along with the substrate-/surface-specific interactions, affects the molecular ordering of the backbone chains as evidenced from FTIR [40], NR

Change in the Properties of Nafion Thin Films relative to their value for Nafion bulk Membrane (25-50 μm)
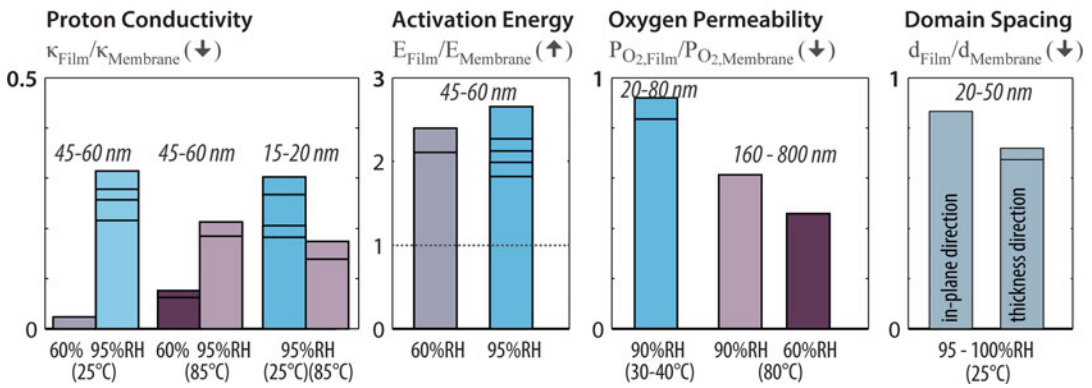
Ionomer Thin Films in PEM Fuel Cells, Fig. 4 Relative change in properties of a Nafion thin film with respect to its value for thicker Nafion membrane under the same conditions. Values are determined based on the reported values for proton conductivity and activation energy for conductivity (using interdigitated substrates) [34, 35, 37, 64, 67], oxygen permeability (from microelectrode studies) [25, 28, 65], and GISAXS [20, 24] data, where orientation of the backbone chains and ionic domains resulted in reduced water uptake [27, 33, 57, 62] and transport processes [27, 33, 57, 62]. The increase in ionomer's transport resistance under confinement can be explained by the changes in swelling and morphology of the thin film, as described in the following sections.

[8, 13, 39], and hydrophilic-domain spacing (from GISAXS) [24]. Thickness values of films are matched and grouped together, but the substrates could differ among the studies due to the distinct nature of setups and techniques used to probe each property. (Values from different reports are shown as individual bars plotted together for similar thicknesses.)

Swelling and Sorption Behavior

A key driving force behind an ionomer's structure/property relationship is hydration. Owing to their hydrophilic nature, the ionic moieties absorb water molecules from the surrounding humid environment. The amount of water in the hydrated ionomer is usually quantified by the local *water content*, λ (= mol H_2O/mol SO_3^-) [74], which is described as

$$\lambda \equiv \frac{n(H_2O)}{n(SO_3)} = \left(\frac{M_w}{M_p}\right)\frac{\overline{M}_p}{\overline{M}_w}, \text{ and} \qquad (1)$$
$$\overline{M}_p = EW = \frac{1}{IEC}$$

where $M_{i(=w,p)}$ and $\overline{M}_{i(=w,p)}$ are the mass and molar mass of phase i, respectively, and the subscripts w and p stand for water and dry polymer, respectively. The degree of sulfonation in PFSA ionomers is commonly represented by the equivalent weight (EW), which is inversely proportional to the ion exchange capacity (IEC). The ionomer accommodates the absorbed water molecules in its hydrophilic nano-domains, which grow with hydration and separate from the hydrophobic polymer backbone. Thus, hydration drives the ionomer's phase-separated nanostructure, which results in a volumetric swelling at macroscopic level. The volume change at a given RH with respect to dry state can be related to dimensional change in each direction (i), L_i/L_{dry}, as follows:

$$\frac{V_{dry} + V_w}{V_{dry}} = \left(\frac{\overline{V}_{dry} + \Delta\lambda\overline{V}_w}{\overline{V}_{dry}}\right) = \prod_i \frac{L_i(\lambda)}{L_{dry}}$$
$$\equiv \left(1 + \frac{L_{iso}(\lambda)}{L_{dry}}\right)^m, \qquad (2)$$

where $\overline{V}$ represents the molar volume. If one assumes isotropic swelling, $L_i(\lambda) = L_{iso}(\lambda)$, then a simplified expression could be obtained for swelling as a function of λ. In the expression above, the swelling dimension, m, takes the value of 3 for three-dimensional (3-D) swelling.

The water uptake and swelling of PFSA membranes are well established based on measurements at a controlled water vapor activity, a_w (or relative
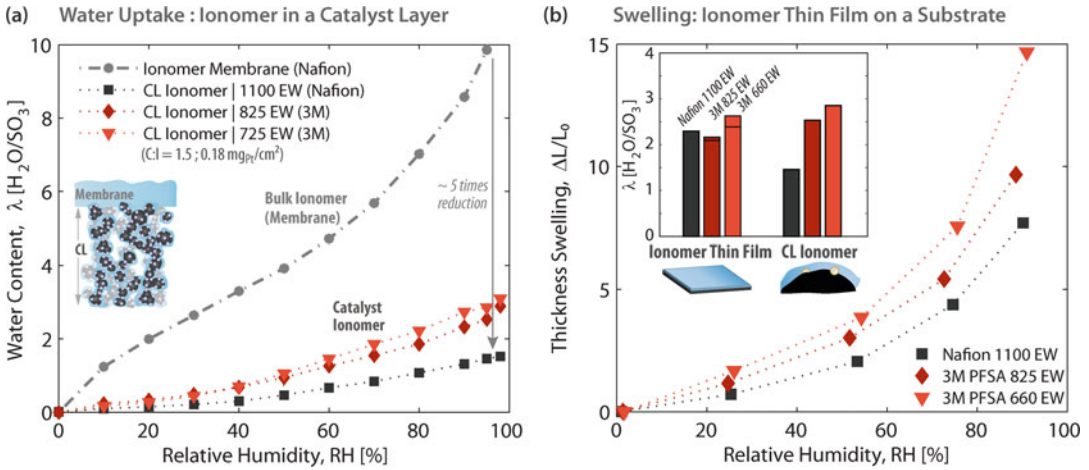
Ionomer Thin Films in PEM Fuel Cells, Fig. 5 Comparison of (**a**) water uptake behavior of catalyst layer (CL) ionomer (measured without the membrane) and (**b**) ionomer thin films of 50 nm spin cast on silicon substrate, measured at 25 °C. The ionomers are 1100 EW Nafion and 825 and 725 EW 3 M PFSAs. Water uptake profile for bulk Nafion 212® membrane was included in (**a**) for comparison. The inset in (**b**) shows the water content at 95% RH converted from the uptake and swelling data for CL ionomer and for thin films, respectively

humidity, RH), at a given temperature [75]. Hydration behavior of PFSA thin films is usually characterized using quartz crystal microbalance (QCM) and ellipsometry (Fig. 2). While QCM determines the mass change of a thin film on a quartz crystal substrate based on the change in sample frequency during hydration, ellipsometry measures the thickness swelling, $\Delta L/L_0$, of a film by measuring the change in its optical response. PFSA thin films' mass uptake can be characterized by QCM using the Sauerbrey analysis, which determines the mass change in the film during hydration, ΔM, from the resonance frequency change, Δf, of the quartz crystal [20, 25, 30, 32, 33, 55, 69]. Such analysis holds for ionomer films of less than 600 nm where they do not exhibit dissipation or viscoelastic losses [33, 55]. Ellipsometry also provides properties such as the refractive index of the ionomer, which must be modeled to determine the film thickness. The wavelength dependence of the refractive index $n(\lambda_{\text{wave}})$ is analyzed using the Cauchy model [31, 76]:

$$n(\lambda_{\text{wave}}) = A + \frac{B}{\lambda_{\text{wave}}{}^2} + \frac{C}{\lambda_{\text{wave}}{}^4} \qquad (3)$$

where A, B, and C are coefficients determined through the data modeling. With the above

expression, a thin film is modeled as a Cauchy layer that describes the dispersion of light in transparent media with minimal light absorption and is used to determine the film's thickness.

Figure 5 summarizes hydration behavior of PFSA ionomers as a membrane (PEM), catalyst ionomer film, and thin film. Compared to a bulk membrane, ionomers in the CLs have much lower water content at a given RH. Moreover, as the ionomer IEC increases, the catalyst ionomer's water uptake capacity increases. A similar effect of IEC on ionomer is observed from the thickness swelling data of PFSA thin films on a silicon substrate. In fact, the calculated water content values are comparable for the ionomer films in CL and on a flat substrate, which demonstrates the potential of ionomer thin films as model systems (Fig. 5b).

Comparison of swelling (ellipsometry) and uptake, λ (QCM), values could provide insight into ionomer's hydration behavior [20]:

$$1 + \underbrace{(\lambda)}_{\text{QCM}} \frac{\overline{V}_{\text{w}}}{\overline{V}_{\text{p}}} - \frac{\overline{V}_{\text{mix}}}{\overline{V}_{\text{p}}} = \underbrace{\left(1 + \frac{\Delta L}{L_{\text{dry}}}\right)^m}_{\text{Ellipsometry}} \qquad (4)$$

where the (partial) volume of mixing $\overline{V}_{\text{mix}}$ accounts for the contribution due to nonideal

mixing [77]. A fair approximation for thin films is $m = 1$ as they are confined on the substrate, which allows them to swell only in the thickness direction [27, 32, 33, 36]. Swelling dimension increases toward 2 as the thickness increases over 200 nm, for the fact that in-plane swelling starts as the film's top surface is less restricted by the constraints imposed by the substrate. A value of $m = 3$ should be reached as the ionomer approaches the "bulk" regime. As for $\overline{V}_{mix}$, it is known for bulk membranes that the partial molar volumes change as a function of hydration due to the mechanisms of solvation, although with relatively minor effects at higher hydration levels [75]. In the case of 1-D swelling assumed ($m = 1$), the contribution from nonideal mixing could be negligible ($\overline{V}_{mix} \approx 0$) [27]. Physically, the low volume of mixing effect indicates that confinement alters the solvation process in the ionomer, which is also evident from the shape of the hydration isotherms of thin films (Fig. 5b), which lack the primary solvation regime at low RH (i.e., Langmuir regime for bulk PFSAs). The thin-film uptake curve exhibits lower λ for a given RH than for a bulk membrane. This is especially apparent at higher RHs, where hydration is expected to be driven by entropic effects and not primary solvation [78–80]. Thus, confinement effects not only reduce the swelling of ionomer thin films but also change the nature of the associated water (i.e., whether it is strongly bound to an ionic group or freely moving). Overall, the qualitative trends between QCM and ellipsometry are consistent, with the latter being more commonly employed as it works on most substrates, albeit with the caveat of using the correct model for the data analysis and difficulties with converting swelling to water content [53].

Even though limitations in swelling could occur due to confinement, the reality is more complex due to the interplays among confinement and substrate composition, casting, and ionomer chemistry. The current state of understanding of hydration behavior of PFSA thin films can be summarized as follows [20, 24, 69]:

(i) Ionomer's swelling could be correlated to its water (mass) uptake where a 1-D swelling represents a fair approximation, the accuracy of which, however, decreases with increasing film thickness (from 100s of nm to 1 μm) [20, 24].

(ii) As the film thickness decreases to 50 nm, its swelling continuously reduces relative to its value for thick (bulk) membrane. Once the film is confined to below 15 to 20 nm, however, it enters a different regime with much higher swelling and a stronger dependence on the substrate composition. As an example, swelling of Nafion on Au is comparable on C for 35 to 50 nm thickness, but increases significantly for 16 nm-thick film (Fig. 6).

(iii) Ionomer's swelling increases with increasing IEC (or lower EW) [24], although differences arising from such effects are less pronounced in terms of water content, λ, which, by definition, accounts for the number of SO_3^- groups (see Fig. 5b).

(iv) Swelling of self-assembled thin films is higher than spin-cast films on gold, but the opposite is true on carbon, caused probably by the substrate-specific interactions changing the adsorption of the PFSA moieties from the solution to the substrate during film formation [20].

(v) Thermal annealing reduces water uptake and swelling of thin films [20, 24, 66, 70] and increases crystallinity [24], similar to its effect
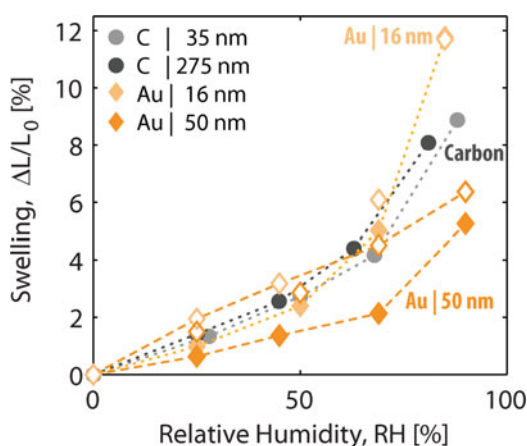
Ionomer Thin Films in PEM Fuel Cells, Fig. 6 Thickness swelling (ellipsometry) data of Nafion thin-film spin casts on carbon and gold substrates (from Ref. [20]). Open and closed symbols correspond to unannealed and annealed films, respectively

on bulk membranes. The impact of annealing is substrate dependent where it decreases with decreasing film thickness on gold but increases on carbon (see Fig. 6), owing to the stronger sulfur interactions with gold than carbon. Thinner films on substrates like Au and Pt are strongly interacting with the substrate surface, which pins the ionic moieties onto the substrate, thereby restricting the motion and conformation changes of ionomer chains under thermal conditions, which is also supported by the morphological evidence (from GISAXS studies[20]).

Hence, when it comes to the effects of processing and substrate, the latter could dominate the ionomer's hydration, especially when it strongly interacts with an ionomer confined to less than 50 nm. Such interactions also drive the changes in T_α [70] and modulus [38], which alter the effect of the thermal treatment process. However, such surface alteration is more restricted in ultrathin films (~10 nm), which require more thermal energy for annealing and therefore a higher annealing temperature. This also explains why the influence of annealing on thin film's hydration changes both with film thickness and substrate.

Morphology

As with their swelling behavior, the phase-separated morphology of PFSAs also changes under confinement and in the presence of substrate and wetting interactions, as evidenced by various techniques including grazing-incidence small-angle X-ray scattering (GISAXS) [20, 24, 27, 53, 57, 62], neutron or X-ray reflectivity (NR or XR) [25, 27–29], TEM [53], spectroscopic techniques (e.g., XPS or FTIR/ATR) [40–46, 81, 82], cryo-TEM tomography [83], fluorescence [33], AFM [53, 56, 67, 69, 70, 84–87], contact angle [45, 64, 67, 70], PM-IRRAS [68], and positron annihilation lifetime (PAL) spectroscopy [45].

GISAXS and NR in particular are powerful tools to investigate the orientation and spatial distribution of the nano-domains, at and below the thin-film interfaces [20, 25, 28, 29, 57, 88, 89]. As opposed to random, isotropic distribution of

domains in bulk PFSA, in thin films, a hydration-dependent lamellar-like nanostructure forms at the film/substrate interface, with alternating layers of water-rich and polymer-rich domains (Fig. 3) [25, 28]. In addition, on hydrophilic substrates (such as SiO_2), a water-enriched surface with a water layer thickness of 1 to 3 nm is observed due to the excess water at the substrate/film interface [25, 69, 89]. Such ordering at the interface could propagate a significant distance (10s of nm) through subsequent layers in a thin film, inducing a locally ordered morphology with alternating layers of SO_3^- rich hydrophilic domains and fluorocarbon hydrophobic domains (Fig. 3) [24, 25, 55, 69, 88, 89]. A recent FTIR study on a PFSA thin film [40] documented different polarizations in and out of the plane of the film, with stronger z-polarized electric field in thinner films indicative of chain alignment parallel to the surface. Such molecular ordering exhibits a transition around 50 nm and depends on processing such as spin casting. The preferential domain alignment is strongest closer to the interface, depending on the substrate interactions, and diminishes along the successive layers toward the film surface [25, 28, 55, 89] (Figs. 3 and 7). Such changes in film morphology with the substrate, along with the impact of thickness and humidity, were also witnessed in GISAXS studies [20, 24]. Typical GISAXS patterns for Nafion films (of 90 ± 10 nm thickness) on various substrates are compared and analyzed in Fig. 7.

Compared to scattering based on transmission (through membranes), techniques for thin films rely on reflection geometry, where the incident beam applied at a shallow incident angle ($\alpha_i \ll 1°$) enters the film and then reflects from the substrate/film interface [90]. To accomplish this, the incidence angle must be lower than that critical angle, α_{cr}, of the film yet lower than that of the substrate, $\alpha_{cr, film} < \alpha_i < \alpha_{cr,substrate}$. Under such *grazing-incidence* conditions, sufficient beam path could be achieved to collect scattering patterns that probe the local structure of a thin film as well as its interface with the substrate. While the reflection geometry increases the complexity of the scattering, it nonetheless provides a powerful method to characterize polymer thin films [90].

Ionomer Thin Films in PEM Fuel Cells, Fig. 7
(a) 2-D GISAXS spectra of 100 nm Nafion thin film on SiO$_2$ substrate at different humidities and the evolution of the ionomer peak obtained from the intensity profile during humidification. (b) Comparison of GISAXS patterns for vapor-saturated (100% RH) Nafion films of two thicknesses on carbon and gold substrates. (c) Impact of thickness and substrate on the orientation parameter of Nafion film, which was calculated from the distribution of intensity along the azimuthal angle at the ionomer peak position (shown schematically below) (Data are compiled from Kusoglu et al. [20, 24]) (For ease of comparison, only one quadrant of the 2-D images is shown due to their symmetry along the vertical axis, q$_z$)

Morphology of Hydrated Nafion Thin Films (GISAXS)

(a) Effect of Humidity

(b) Effect of Substrate
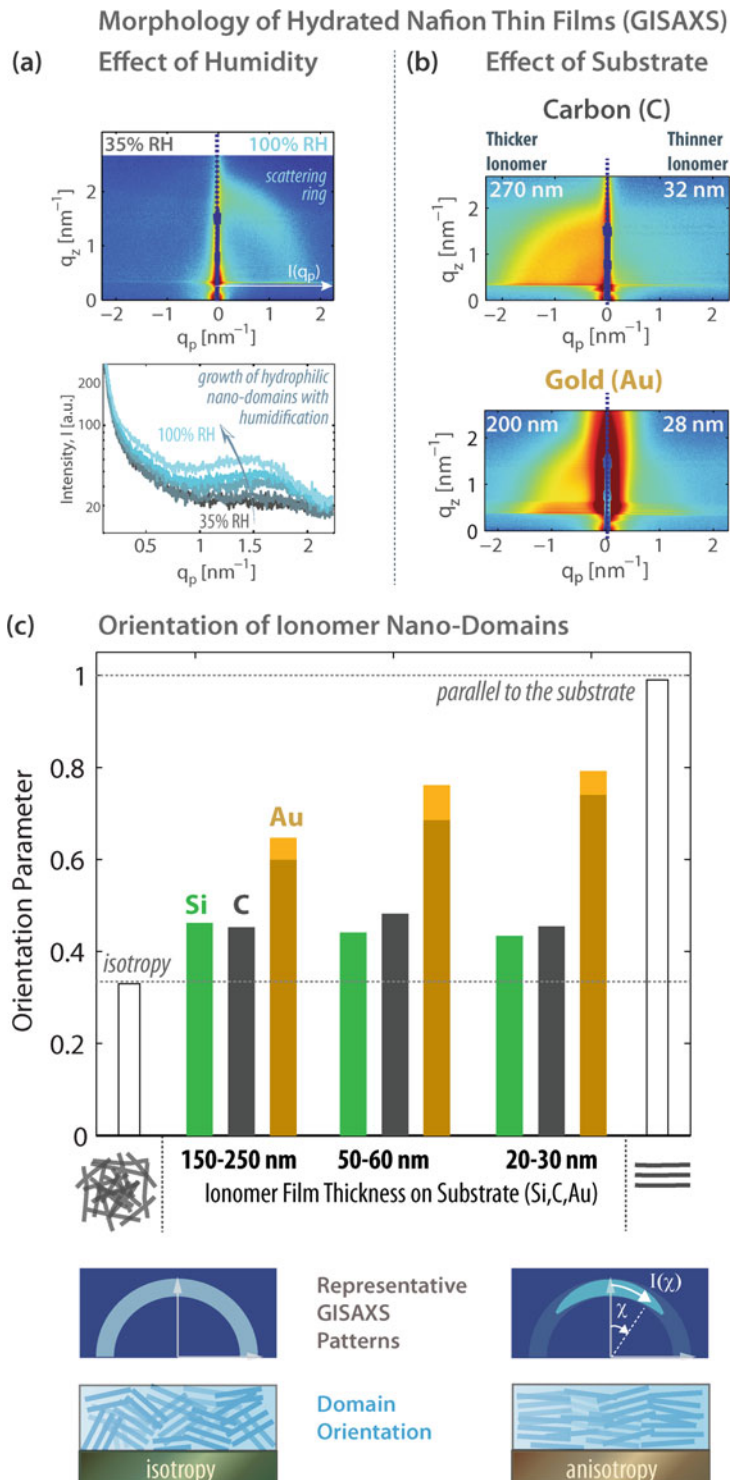
Characteristic features of GISAXS patterns for Nafion thin films shown in Fig. 7 are summarized as follows:

There exists a scattering half-ring that intensifies with humidification indicating hydration-driven phase separation with a correlation length between $q = 1.5$ and 2.5 nm^{-1}, which corresponds to domain spacing of $d = 2\pi/q \approx 2.5$ to 4.5 nm [20, 57]. The degree of phase separation, quantified by the full-width half-max (FWHM) of the ionomer peak, decreases with film thickness and almost disappears for ultrathin films [20, 24, 27, 57]. Nevertheless, this trend is strongly influenced by the IEC (or EW) of the ionomer, increase in which it tends to enhance phase separation at a given thickness due to a higher fraction of ionic moieties [24]. As the film thickness is reduced below 50 nm, the ionomer begins to exhibit weaker phase separation, which is evident from the broader ionomer peak in GISAXS [20, 53, 57], more mixing of smaller-size domains in TEM images [53] and AFM [56], as well as the change from hydrophobic to hydrophilic film surface [45, 67, 70].

A rather more important consequence of confinement is the (nano)structural anisotropy. Scattering patterns begin to exhibit slight deviations from isotropy as the film gets thinner since the ionomer chains are topologically confined. A comparison between the intensity profiles taken parallel (I-q_p) and perpendicular (I-q_z) to the substrate indicates stronger phase separation in thickness direction, accompanied by smaller domain spacing. Compared to the isotropic d-spacing of a bulk-like ionomer, confinement reduces the ionomer's d-spacing more in the thickness direction ($d_z < d_p$) (Fig. 4). Nevertheless, in the thickness direction, ionomer preserves its phase-separated nanostructure aided by the confinement effects, which induce preferential orientation of domains parallel to the substrate. In such a configuration, domain orientation is influenced also by the strength of the substrate/film interactions.

Figure 7b reveals a sharp contrast in PFSA structure between carbon and metallic substrates. PFSA film's nanostructure exhibits closer to a semicircular (isotropic) ionomer peak on silic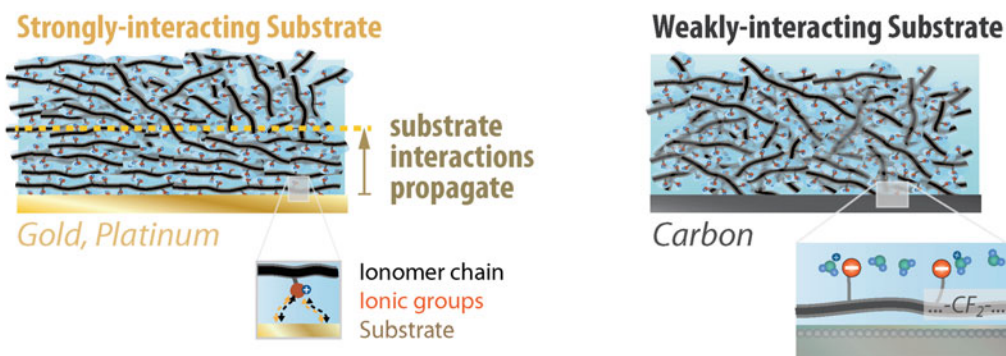on and carbon substrates, whereas it becomes more anisotropic on gold and platinum. Also, the substrate appears to have a stronger impact on domain orientation than on domain spacing. To characterize this nanostructural anisotropy, an *orientation parameter*, O.P., is calculated from the distribution of ionomer peak intensity as a function of azimuthal angle, χ (Fig. 7):

$$O.P. = \left\langle \cos^2\chi \right\rangle$$
$$= \frac{\int_0^{\pi/2} I(\chi)\sin(\chi)\cos^2\chi d\chi}{\int_0^{\pi/2} I(\chi)\sin(\chi)d\chi} \qquad (5)$$
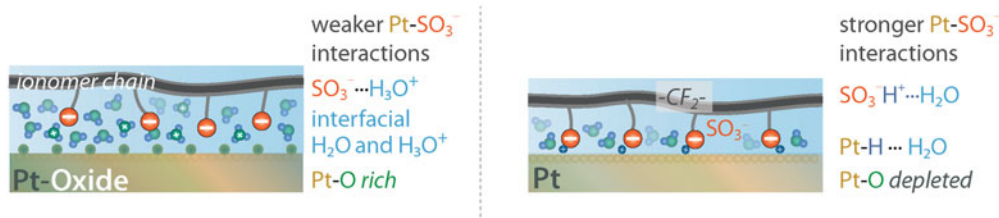
An O.P. of 0 and 1 corresponds to perpendicular and parallel orientations, respectively, while an isotropic distribution of intensity ($I(\chi) = constant$) yields O.P. $= 0.33$. As shown in Fig. 7c, the orientation parameter for Nafion thin film depends both on thickness (confinement) and substrate (interactions), with the latter imposing a stronger effect. On silicon and carbon, the O.P. is closer to the isotropic distribution, regardless of thickness. On gold substrates, however, PFSA films exhibit a stronger orientation accompanied by a secondary impact of thickness. As the ionomer is confined on gold to a thickness below 50 nm, its O.P. approaches 1, which is the theoretical value for parallel alignment. Hence, the strong interactions of PFSA moieties with metallic substrates lead to substrate-induced ordering, which is enhanced under confinement. Thus, for ultrathin films, the substrate-ionomer interaction is strong enough to propagate the entire film leading to preferential alignment of all the domains therein (Fig. 8a).

An increasing number of studies agree on formation of a partially ordered ionomer domain structure closer to the film/substrate interface [20, 28, 33, 38, 45, 55, 67], albeit with a strong substrate dependence [20, 28, 45, 56, 57]. Such alignment in confined geometries is possible in light of recent evidence on the locally flat, ribbon-like morphology of PFSA (see Ref. [75] for additional reading). It was shown that during humidification of PFSA thin films, hydrophilic d-spacing ($d(\lambda)/d_{dry}$) increases with thickness swelling ($L(\lambda)/L_{dry}$) in an affine manner,

(a) Effect of Confinement and Substrate on Ionomer thin-film Nanostructure

Strongly-interacting Substrate

substrate interactions propagate

Gold, Platinum

Ionomer chain
Ionic groups
Substrate

Weakly-interacting Substrate

Carbon

...-CF$_2$-...

(b) Effect of PFSA Ionomer - Substrate Interactions on Local Structure

weaker Pt-SO$_3^-$ interactions

ionomer chain

Pt-Oxide

SO$_3^-$···H$_3$O$^+$
interfacial
H$_2$O and H$_3$O$^+$
Pt-O *rich*

stronger Pt-SO$_3^-$ interactions

-CF$_2$-
SO$_3^-$
Pt

SO$_3^-$H$^+$···H$_2$O
Pt-H ··· H$_2$O
Pt-O *depleted*

Ionomer Thin Films in PEM Fuel Cells, Fig. 8 (**a**) Impact of substrate interactions on the local orientation of PFSA domains on weakly and strongly interaction substrates. (**b**) Changes in the nature of Pt/ionomer interface under oxidizing and reducing environment

indicative of locally flat domains [24]. Hence, a bulk PFSA ionomer can also be interpreted as a mesoscale assembly of ionomer structures with local order, like thin films, which could also serve as a model constituent for studying multi-scale transport phenomena.

From these studies, a morphological picture for PFSA thin film emerges where the ionomer domains have stronger packing and preferential orientation nearby the substrate. In the plane of film, however, they maintain their interconnected network with more random orientation. It is instructive to consider that close packing of domains also results in a strong densification of ionomer, thereby giving rise to additional resistance to the transport species perpendicular to the substrate. In such a confined geometry, the polymer chains do not have sufficient energy to orient themselves randomly as they do in a bulk volume, and therefore exhibit preferential alignment,

thereby impacting transport of ions [5, 35–37, 53, 91], water [20, 32, 65, 68, 73], and gases [6, 8, 15, 39]. It should be noted that ionomer chains still have relatively more conformational freedom in the plane, where their mobility is less likely to be restricted compared to that perpendicular to substrate.

In accord with these morphological changes, the surface of a PFSA thin film also changes under confinement, which is probed by methods such as contact angle measurements and electrochemical AFM. The contact angle of a Nafion film exhibits a strong dependence on not only the thickness but also the thermal history. Below a critical thickness, L_{cr}, the film surface is hydrophilic and becomes more hydrophobic as the thickness increases toward bulk-like values (L > L$_{cr}$) [31, 64, 67]. The contact angle of a Nafion film decreases from 100° to almost 0° around a critical thickness of $L_{cr} = 50$ to 60 nm and then increases

slightly up to 20° for a film of a few nanometer [31, 64, 67]. The hydrophilicity of thin-film surface was also confirmed by PALS, showing an SO_3-rich surface [45] and NMR [87], which demonstrated that the local hydrogen-bonding structure of a 10 nm film is water rich with a high dissociation of protons and exhibits no further change in ^1H chemical shifts and mobility with temperature [87]. This is in contrast with a 160-nm-thick film, which exhibit a bulk-like behavior with a temperature-dependent proton mobility, and thus does not suffer from the kinetically trapped state with limited mobility that ultrathin films experience [87]. In addition, a Nafion film annealed at C exhibits hydrophobic surface, regardless of the thickness [70]. However, once an annealed film is exposed to liquid water, it becomes hydrophilic again, signifying a surface reorganization that can be switched by means of surface treatments, accompanied by changes in surface roughness [64, 70]. The fact that switching of the surface wettability requires a higher annealing temperature for thin(ner) films indicates the highly restrictive mobility of Nafion as its confinement increases.

Structure/Property Relationship and Transport

It is clear that a thin film's internal and surface morphology poses significant limitations to transport and overall device performance [7, 27, 33, 56, 57, 62, 65, 91]. Due to similar transport limitations between the Nafion electrolyte films formed in PEFC electrodes [6, 7, 9, 11, 14, 18, 92] and Nafion thin films [20, 27, 32, 33, 36, 57, 91], thin films are used as model systems to investigate and model electrode ionomers [1, 2, 7]. Key for electrode performance is good oxygen permeability with proton conductivity across/through an ionomer thin film on and between carbon/Pt agglomerates. Since both transport properties tend to deteriorate for nm-thick films, understanding the structure/transport properties therein is of great importance. As discussed above, such transport resistance, while being driven by the confinement, is also impacted by the ionomer/Pt interaction, with structural ordering through chemical affinity of SO_3^- groups onto Pt. With the formation of water-

enriched surfaces near the substrate, which was evidenced by the availability of non-H-bonded water [43] it becomes easier to solvate SO_3 groups with lower energy cost on backbone chain's deformation. In a DPD model of a 10-nm-thick Nafion on carbon, diffusion was found to be anisotropic, higher along the film and lower in thickness direction [93]. Similarly, the conductivity of ionomer films along the ionomer-substrate interface is strongly influenced by the molecular orientation and ordering of the ionomer moieties therein [91]. Thus, the impact of morphological changes on transport is largely dependent on the direction on which the mechanism is probed.

Confinement-driven structural changes and ordering reduce not only the transport properties but also their kinetics. For example, swelling kinetics of thin films have been shown to yield time constants [18, 20, 32, 57, 65] similar to those found for the interfacial transport of bulk membranes, thus revealing the thin-film nature of bulk-membrane interfaces. It must be noted, however, that correlating kinetic effects with confinement is not trivial, especially when probing transport parallel or perpendicular to the substrate. This is because swelling kinetics is strongly intertwined to dynamic of morphological changes, such as formation of interfacial layering [25, 65]. It is worth noting that similar phenomena occur at the open surface of an ionomer, where the humidity-dependent film interface changes the mass transport and its kinetics [59, 61, 94, 95]. An intriguing consequence of this phenomenon is observed when gas transport at the film's interface is probed electrochemically using a Pt electrode, where the electrochemically generated water changes the interface, thereby affecting the measured property and its kinetics [59].

Hence, there exists a strong interplay between the film's morphology and transport phenomena, as dictated by confinement and interactions, whether it is in contact with air or a substrate [8, 14, 20, 34, 53, 55, 67, 68]. When confined to thin films, PFSA exhibits not only lower diffusion [27, 54, 65, 68, 71, 72] but also a few orders of magnitude slower relaxation, indicating more restricted chain dynamics [68]. An important implication of confinement effect for fuel cell

ionomers is the reduced conductivity with decrease in film thickness [5, 34, 36, 37, 53, 64, 70, 91] and substrate dependence [34] (Fig. 4), which can be associated with decreased water uptake [34, 36, 64, 70, 91] and the number of conducting sites (from conductive AFM) [56], as the conductivity-λ relationship was shown to extend to the thin-film regime, albeit with differences from that in the bulk regime [69]. Concurrent with the confinement-driven increase in resistance to transport of water and ions, activation energy for conductivity also increases as the film thickness is reduced [34, 35, 37, 64, 67, 91] (Fig. 4). Conductivity of PFSA film decreases also after thermal annealing, the impact of which, however, diminishes for ultrathin (10 nm) films, which exhibit minimal rearrangement in response to heat-treatment processes [35]. A noteworthy observation is that the reduction in conductivity upon heat treatments is more pronounced than that in swelling, which not only reveals the key roles of morphological changes and film interactions on transport resistances [20, 64, 70] but also underscores the enthalpic and entropic contributions to chain dynamics in thin films which are controlled by both kinetic and thermodynamic phenomena.

Similar to conductivity, oxygen permeability also decreases in thin films [6, 8, 13, 15, 39]. Oxygen transport in thin films is measured electrochemically using a microelectrode setup, where one of the dimensions of the Pt electrode is small enough to probe local resistances at the ionomer/Pt interface during oxygen reduction reaction (ORR), thereby mimicking the mechanisms occurring in PEFC cathodes [8, 39, 59, 96–98]. By sweeping potential under various concentrations of O_2, diffusion-limited current densities are achieved and used to relate for various film thicknesses to the O_2 transport through the film to the interface. With such characterization, one can identify the contributions to the O_2 transport resistance in CLs (shown in Fig. 1) and study the role of ionomer film. However, such analysis is nontrivial due to the nanometer thicknesses probed. Kudo et al. [8, 39] showed that the reduced O_2 permeation in thinner films exhibits a thickness dependence, which is governed by the surface interactions of the film, especially at the Pt/ionomer interface. While an overall interfacial resistance to

gas transport is inferred, separating the oxygen permeation through ionomer's inner regions and at the ionomer/Pt layer is difficult as below 20 nm thicknesses, the entire ionomer film exhibits densification and acts as an "interface."

Furthermore, any preferential alignment is expected to result in local stiffening, which was evidenced by fluorescence showing anti-plasticization [33] and correlates to the observed increase in the modulus of thin films [26, 38]. These changes are consistent with the reduced water uptake due to a stronger mechanical force in the mechanical/chemical energy balance that controls swelling equilibrium. One potential strategy for altering this balance and overcoming transport limitations is using PFSAs with higher IECs and different side chain chemistries. Lowering the EW of a PFSA ionomer film increases its swelling, which could be favorable for enhancing some of the transport mechanisms, but it could also increase the local order near the Pt substrate (Fig. 8b), thereby affecting the transport of species to that interface. For example, MD simulations showed that increasing the side chain density by lowering the EW enhances the H-bonding and charge-dipole interactions, which impedes water mobility and its self-diffusion [99]. Such an effect is explored in CLs, where low-EW ionomers could increase O_2 transport resistance despite absorbing more water [15]. Thus, changes in ionomer's side chain chemistry and density in the presence of an interacting substrate could significantly alter the transport mechanisms, which result in multiple distinct factors influencing the film's swelling and transport properties and making it challenging to establish their underlying origin.

Substrate/Film Interactions and Related Phenomena

The nature and composition of the substrate surface, including its oxide layers (e.g., SiO_2, PtO), is critical to the understanding of their interactions and response to various stimuli, such as humidity and electrochemical potential [8, 19, 20, 29, 30, 34, 41, 56, 69, 91, 100, 101]. Thus, compared to a hydrophilic Si native-oxide surface, films on hydrophobized Si substrates exhibited less water uptake and strong structural anisotropy with

domains parallel to the substrate [57]. On carbon, the nature of the substrate becomes critical as well [10, 20, 29, 30, 45, 56]. In addition, aging of carbon was shown to cause surface oxidation and rearrangement, accompanied by reduced film thickness and irreversible swelling [29]. Also, when the carbon surface is hydrophobic, the ionomer's interactions occurs via its apolar fluorocarbon chains [10], whereas hydrophilic carbon preferentially interacts with the polar SO_3H groups (Fig. 8a) [102]. Similarly, aggregates of PFSA are randomly adsorbed onto a highly oriented pyrolytic graphite (HOPG) surface, thereby forming an ordered morphology [103]. The favorable interactions between SO_3^- groups and a hydrophilic substrate's polar groups [29, 45, 56, 57, 103] become strongest on a Pt substrate [41, 45, 56, 101] (Fig. 8). While the NR studies report higher affinity of SO_3^- groups on hydrophilic SiO_2 compared to metallic substrates [25, 28], GISAXS data show stronger substrate-induced morphological changes on Au and Pt [20], which is likely the cause of stronger domain orientation (Fig. 8c). Nevertheless, due to dynamic and chemically heterogeneous nature of the substrate-ionomer interface, local structure probed therein could also be influenced by the type of excitation, which could explain some of these discrepancies between various techniques. The substrate-specific changes are in accord with simulation results [43, 93, 104–106], confirming the key role of affinity of water to the substrate in an ionomer's molecular rearrangement that affects the morphology [104] and surface hydrophilicity [70, 93, 104, 105].

PFSA($-SO_3H$)/Pt interactions are well-explored electrochemical cell studies to elucidate the effects of electrochemically formed water and the oxide layer formation on ionomer film behavior [6, 8, 14, 29, 30, 44, 101, 107] with spectroscopic evidence [41–44] and supported by molecular simulations [43, 104, 106] (Fig. 8b). These studies confirmed the high chemical affinity of sulfonate SO_3^- groups to the Pt, which was also supported by FTIR [41, 43, 44], XPS [45], PALS [45], and MD studies [10, 43, 99, 104, 108]. PFSA/Pt interactions were shown to be reversible during Pt-oxide formation and reduction such that

adsorption of PFSA moieties onto the Pt surface weakens and disrupts surface oxide formation (e.g., due to applied electrochemical potential) [14, 30, 41, 44, 101, 107]. Thus, in reducing environment as well as at low hydration levels, PFSA's acid groups are embedded on the Pt surface, whereas formation of an oxide layer (PtO) creates a polar, hydrophilic interface between the ionic groups and the Pt particles [41, 44]. Such changes affect the long-range restructuring of the ionomer chains, which was accompanied by the changes in the mobility of SO_3^- H_3O^+ and H_2O [41, 44], ionomer structure [14, 30, 41, 43, 45, 101], and transport resistances [6, 8, 14, 29]. Spectroscopic evidence suggests that with increasing potential, SO_3^- preferably adsorbs onto the Pt, which restricts the vibrational mobility of ionic groups (vs- (SO_3^-)) and expels the water molecules from the interface [41]. Cyclic voltammetry (CV) studies showed that the SO_3^- adsorption/desorption peaks are shifted to lower potentials with ionomer dehydration indicating enhanced adsorption of SO_3^- onto Pt under drier conditions, which is attributed to higher local concentration of SO_3^- and/or reduced hydration stabilization energy of ionomer [14, 109]. Hence, strong ordering of ionomer chains at the interface aided by the Pt-SO_3^- interactions restrict the mobility of the pendant chains and reduce the fraction of available (active) ionic groups participating in transport, which could effectively block the gas transport pathways and thereby increase the local O_2 resistance [7, 8, 11, 14, 15]. This phenomenon is also interpreted as the poisoning effect of the ionomer on the catalyst. The adsorption/desorption of the SO_3^- onto/from the Pt could be explained by the balance between an electrode metal spring (Pt-SO_3^-) and ionomer spring (backbone-SO_3-cation) [101]. With increasing potential, SO_3^- approaches Pt, as the Pt-SO_3^- interaction dominates the cation/anion interaction within Nafion. For the same reason, for other cations that interact more strongly with SO_3^-, a higher activation potential is needed to adsorb the cations onto the electrode surface [101]. Thus, in essence, SO_3^- responds to electric potential like single counterions (i.e., forming an electric double layer) [44] and affects the backbone (orientation)

through the flexible side chain [43, 44, 108]. These interactions also change the nature of interfacial water, some molecules of which are relocated to Pt, thereby reducing the hydration of the sulfonate layers (i.e. less H_3O^+) and hydrogen bonding [43, 107, 108]. Therefore, the potential- and hydration-dependent changes of the Pt surface, including its oxide coverage, influence, chemically, the interaction and mobility of the ionomer's acid groups and, physically, the densification of the ionomer at the interface, which together controls the diffusion pathways. This phenomenon was simulated in a MD study, which showed that closer to the Nafion/substrate interface, the ionomer density increases, but its O_2 concentration decreases [106].

Summary and Remarks

In summary, from the current state of understanding of PFSA thin films, the following thickness regimes can be identified (see Fig. 3):

(i) *Bulk-like regime*: (from μm down to a few 100 nm) where the majority of ionomer volume behaves like the inner regions of the bulk membrane, albeit still with interfacial effects arising from the presence of a surface layer which may differ from the inner structure.

(ii) *Thin-film regime*: (between O (10) nm to a few 100 nm) where confinement-induced changes begin to influence the structure/transport properties resulting in reduced swelling, slower diffusion, limited transport properties, and anisotropic nanostructure with preferential orientation of ionomer domains parallel to the substrate. Such confinement-driven orientation also enhances the role of substrate/film interactions, which could induce additional changes in morphology including local ordering of the domains at the substrate/film interface, accompanied by higher transport resistances therein.

(iii) *Ultrathin-film regime*: (less than 20 nm) where the ionomer interactions with the substrate and open surface cause an intriguing interplay that propagate throughout the film thickness. As the film thickness approaches the characteristic length scale of the ionomer (e.g., domain spacing), the ionomer begins to exhibit reduced phase separation accompanied by increased swelling, resulting in dispersion-like behavior. In the presence of a metallic substrate, strong alignment and densification of ionomer chains at the substrate interface occurs. In such a morphology, the ionomer might begin to lose characteristic features of its mesoscale domain network, with weaker connectivity between its constituent domains and reduced hydrophobic-domain elastic forces, which tend to prevent dissolution of the ionomer [53].

Although the transitions between these regimes are neither well defined nor understood, there still appears to be a *critical thickness* of 50 to 60 nm, around which confinement effects manifest themselves even stronger as discussed above. It must be noted that this critical thickness (or transitions between regimes) could change in the presence of other effects, such as annealing and substrate interactions, and additional deviations might occur for properties that may be dominated by larger-scale morphological reorganization, such as diffusivity, permeability, and mechanical properties. Similarly, for the bulk-like regime (i), QCM and ellipsometry data deviate the most, suggesting that the swelling and water uptake processes are more complicated due to the presence of additional mixing effects, multidimensional swelling, and disruption of locally ordered structure or its diminishing influence over larger thicknesses.

Due to their similarity to the locally hydrated nano-domains of bulk ionomers and their interfacial layers, thin films show premise for modeling ionomer systems and studying their structure/property relationship at multiple length scales. Hence, a bulk PFSA ionomer can also be interpreted as a mesoscale assembly of ionomer structures with local order, like thin films. Thin films possess a higher level of complexity due to

the presence of electrostatic interactions arising from ionic groups responsive to environments, surface and wetting interactions, and confinement. Thus, additional studies are needed to understand how electrochemical potential impact thin-film morphology and properties in these regimes.

Lastly, for a given substrate composition, the impact of EW and chemistry on ionomer's structure/property relationship is stronger in regime (ii), where shorter backbone chain (lower EW) and side chain collectively enhance the structural order and the degree of phase separation in thin films. The effects of EW in PFSAs are more pronounced in the thin-film regime (ii), which underlies the important role of ionic interactions on the morphology. Since the ionomer interacts via its pendant chains and SO_3^- acid groups, higher IEC could amplify the overall impact of the interactions near the substrate interface thereby enhancing ordering and densification.

Future Directions

The role of ionomers in state-of-the-art PEFCs has expanded beyond the conventional solid electrolyte separator PEM into catalyst layers, where they maintain their electrolyte functionality as a thin film but also require permeation of reactant gases critical for the electrochemical reactions. In particular, the local resistance to oxygen flux at the CL ionomer/Pt interface leads to significant losses in cell performance, especially at reduced Pt loadings. To overcome the performance limitations without sacrificing cost, one must understand the genesis of the transport resistances in the cell, from membrane to CLs. Thus, ionomer thin films serve as model systems to study, characterize, and understand ionomer behavior in PEFC CLs, where transport resistances imposed by confinement and substrate interactions lead to increased mass-transport limitations. Despite the simplified nature of the thin films on model substrates, they help elucidate properties of CL ionomers and pave the way to mimic their behavior under conditions relevant to cell environment with operando characterization techniques. The

fact that both CL ionomers and ionomer thin films exhibit similar water uptake behavior and trends in terms of restrictions to ion and gas transport suggests that thin films can be used as proxies for the films occurring with the CLs. Nevertheless, there exist significant knowledge gaps in terms of (i) improving model systems with more realistic substrate compositions that enable a better representation of the catalyst ionomer films; (ii) investigation under conditions relevant to PEFC operating environment, including humidity, temperature, time, and potential effects; (iii) characterization of the dynamic nature of the substrate/film interfaces, in particular with ionomer/ Pt interactions; and (iv) establishing the structure-property correlations by accounting for ionomer chemistry to model and predict the transport limitations.

In ionomer thin films, the interplay between the interactions and confinement results in preferential orientation and densification of domains, which could pose significant limitations to transport of species occurring through these domains. Most of these transport limitations manifest themselves in terms of reduction in water uptake and diffusion, ion conductivity, and gas permeability, accompanied by higher activation energy barriers. The magnitude of these transport-property reductions changes with many factors, including solvent type, casting and processing conditions (e.g., posttreatment), ionomer chemistry, film thickness, substrate type, composition, and interface, as well as environmental conditions relevant to cell operation (e.g., humidity, temperature, potential), resulting in a wide material parameter space that still remains to be explored fully in order to elucidate the governing phenomena and develop material solutions.

There is a growing body of evidence on changes in PFSA thin films' swelling, water uptake, and morphological features under confinement, which help understand the role of thickness and, to a certain extent, the substrate. Hitherto, most studies on PFSA thin films have focused on silicon substrates, followed by gold. Nevertheless, to better understand the PEFC CL ionomers, there is a need to explore their behavior on carbon- and platinum-mixed substrates and in

thinner regimes. A large fraction of the ionomer films in CLs are below 15 nm thick, yet their structure/function relationship has not been established in model systems, due in part to the challenges associated with probing their morphology and properties at such thicknesses. Furthermore, since thin films exhibit anisotropy in morphology and transport properties, there is a need to explore and model the anisotropy of properties. The thin films highlight the importance of substrate interactions, especially their dynamic nature during operation, such as the formation and reduction of oxide layer on Pt, which expands the required data, needs, and science, most of which are still in early stages. Even though substrate-specific interactions control the ionic moieties' distribution at the interface, a complete picture as to how these interactions control the orientation of ionomer's side and main chain, and their conformation in the morphology propagates through the thickness, has yet to emerge. In particular, there is a need to explore PFSA ionomers beyond Nafion to identify the role of EW and side chain chemistry in controlling thin film's interactions with various substrates and structure/functionality. The fact that permeability of a gas depends on its solubility and diffusion, which respond differently to the environmental and nanostructural changes, makes it difficult to identify the role of chemistry on gas transport near the ionomer/Pt interface.

PFSA ionomers' remarkable transport properties could be associated with its nanoscale environment, where high mobility of bulk-like water aids rapid water and ion transport, and the interconnected mesoscale domain network that governs the macroscopic transport. It is important to understand how this multiscale three-dimensional morphology is disrupted when the ionomer is confined to nanometer thicknesses including anisotropy formation and altered transport properties of various species, which are highly coupled. Moreover, elucidation of the anisotropy in relation to the film's confined domain network requires models and techniques that enable characterization of transport properties beyond scalar values to direction-dependent vectors Thus, there is a need to build a new knowledge base for PEFC

ionomers, to understand their structure/functionality across the length scales, and in the presence of various dynamic interactions. This is a significant challenge and opportunity to design and implement advanced characterization techniques to probe ionomer-substrate interface and to develop more predictive multiscale models to elucidate transport phenomena.

Bibliography

Primary Literature

1. Weber AZ, Kusoglu A (2014) Unexplained transport resistances for low-loaded fuel-cell catalyst layers. J Mater Chem A 2(41):17207–17211
2. Holdcroft S (2014) Fuel cell catalyst layers: a polymer science perspective. Chem Mater 26(1):381–393
3. Soboleva T, Malek K, Xie Z, Navessin T, Holdcroft S (2011) PEMFC catalyst layers: the role of micropores and mesopores on water sorption and fuel cell activity. ACS Appl Mater Interfaces 3(6):1827–1837
4. Lopez-Haro M et al (2014) Three-dimensional analysis of Nafion layers in fuel cell electrodes. Nat Commun 5:5229. doi:10.1038/ncomms6229
5. Siroma Z, Ioroi T, Fujiwara N, Yasuda K (2002) Proton conductivity along interface in thin cast film of Nafion (R). Electrochem Commun 4(2):143–145
6. Iden H, Ohma A, Shinohara K (2009) Analysis of proton transport in pseudo catalyst layers. J Electrochem Soc 156(9):B1078–B1084
7. Kongkanand A, Mathias MF (2016) The priority and challenge of high-power performance of low-platinum proton-exchange membrane fuel cells. J Phys Chem Lett 7(7):1127–1137
8. Kudo K, Jinnouchi R, Morimoto Y (2016) Humidity and temperature dependences of oxygen transport resistance of Nafion thin film on platinum electrode. Electrochim Acta 209:682–690
9. Iden H, Sato K, Ohma A, Shinohara K (2011) Relationship among microstructure, ionomer property and proton transport in pseudo catalyst layers. J Electrochem Soc 158(8):B987–B994
10. Ohma A et al (2011) Analysis of proton exchange membrane fuel cell catalyst layers for reduction of platinum loading at Nissan. Electrochim Acta 56(28):10832–10841
11. Mashio T, Iden H, Ohma A, Tokumasu T (2017) Modeling of local gas transport in catalyst layers of PEM fuel cells. J Electroanal Chem 790:27–39
12. Shinozaki K, Morimoto Y, Pivovar BS, Kocha SS (2016) Suppression of oxygen reduction reaction activity on Pt-based electrocatalysts from ionomer incorporation. J Power Sources 325:745–751
13. Suzuki T, Kudo K, Morimoto Y (2013) Model for investigation of oxygen transport limitation in a

polymer electrolyte fuel cell. J Power Sources 222:379–389

14. Jomori S, Komatsubara K, Nonoyama N, Kato M, Yoshida T (2013) An experimental study of the effects of operational history on activity changes in a PEMFC. J Electrochem Soc 160(9):F1067–F1073

15. Ono Y, Ohma A, Shinohara K, Fushinobu K (2013) Influence of equivalent weight of ionomer on local oxygen transport resistance in cathode catalyst layers. J Electrochem Soc 160(8):F779–F787

16. Morawietz T, Handl M, Oldani C, Friedrich KA, Hiesgen R (2016) Quantitative in situ analysis of ionomer structure in fuel cell catalytic layers. ACS Appl Mater Interfaces 8(40):27044–27054

17. Soboleva T et al (2010) On the micro-, meso- and macroporous structures of polymer electrolyte membrane fuel cell catalyst layers. ACS Appl Mater Interfaces 2(2):375–384

18. Kusoglu A, Kwong A, Clark KT, Gunterman HP, Weber AZ (2012) Water uptake of fuel-cell catalyst layers. J Electrochem Soc 159(9):F530–F535

19. Iden H, Ohma A (2013) An in situ technique for analyzing ionomer coverage in catalyst layers. J Electroanal Chem 693:34–41

20. Kusoglu A et al (2014) Impact of substrate and processing on confinement of Nafion thin films. Adv Funct Mater 24(30):4763–4774

21. Kim TH, Yi JY, Jung CY, Jeong E, Yi SC (2017) Solvent effect on the Nafion agglomerate morphology in the catalyst layer of the proton exchange membrane fuel cells. Int J Hydrog Energy 42(1):478–485

22. Kim YS et al (2015) Origin of toughness in dispersion-cast Nafion membranes. Macromolecules 48(7):2161–2172

23. Welch C et al (2012) Nafion in dilute solvent systems: dispersion or solution? ACS Macro Lett 1(12):1403–1407

24. Kusoglu A, Dursch TJ, Weber AZ (2016) Nanostructure/swelling relationships of bulk and thin-film PFSA ionomers. Adv Funct Mater 26(27):4961–4975

25. Kim S et al (2013) Surface-induced nanostructure and water transport of thin proton-conducting polymer films. Macromolecules 46(14):5630–5637

26. Page KA et al (2015) In situ method for measuring the mechanical properties of Nafion thin films during hydration cycles. ACS Appl Mater Interfaces 7(32):17874–17883

27. Eastman SA et al (2012) Effect of confinement on structure, water solubility, and water transport in Nafion thin films. Macromolecules 45(19):7920–7930

28. Dura JA, Murthi VS, Hartman M, Satija SK, Majkrzak CF (2009) Multilamellar interface structures in Nafion. Macromolecules 42(13):4769–4774

29. Wood DL, Chlistunoff J, Majewski J, Borup RL (2009) Nafion structural phenomena at platinum and carbon interfaces. J Am Chem Soc 131(50):18096–18104

30. Masuda T, Sonsudin F, Singh PR, Naohara H, Uosaki K (2013) Potential-dependent adsorption and desorption of perfluorosulfonated ionomer on a platinum electrode surface probed by electrochemical quartz crystal microbalance and atomic force microscopy. J Phys Chem C 117(30):15704–15709

31. Paul DK, Fraser A, Karan K (2011) Understanding the ionomer structure and the proton conduction mechanism in PEFC catalyst layer: adsorbed Nafion on model substrate. ECS Trans 41(1):1393–1406

32. Kongkanand A (2011) Interfacial water transport measurements in Nafion thin films using a quartz-crystal microbalance. J Phys Chem C 115(22):11318–11325

33. Dishari SK, Hickner MA (2012) Antiplasticization and water uptake of Nafion thin films. ACS Macro Lett 1(2):291–295

34. Ono Y, Nagao Y (2016) Interfacial structure and proton conductivity of Nafion at the Pt-deposited surface. Langmuir 32(1):352–358

35. Paul DK, McCreery R, Karan K (2014) Proton transport property in supported Nafion Nanothin films by electrochemical impedance spectroscopy. J Electrochem Soc 161(14):F1395–F1402

36. Paul DK, Fraser A, Karan K (2011) Towards the understanding of proton conduction mechanism in PEMFC catalyst layer: conductivity of adsorbed Nafion films. Electrochem Commun 13(8):774–777

37. Siroma Z et al (2009) Depression of proton conductivity in recast Nafion (R) film measured on flat substrate. J Power Sources 189(2):994–998

38. Page KA et al (2014) Confinement-driven increase in ionomer thin-film modulus. Nano Lett 14(5):2299–2304

39. Kudo K, Morimoto Y (2013) Analysis of oxygen transport resistance of Nafion thin film on Pt electrode. ECS Trans 50(2):1487–1494

40. Zimudzi TJ, Hickner MA (2016) Signal enhanced FTIR analysis of alignment in NAFION thin films at SiO2 and au interfaces. ACS Macro Lett 5(1):83–87

41. Hanawa H, Kunimatsu K, Watanabe M, Uchida H (2012) In situ ATR-FTIR analysis of the structure of Nafion-Pt/C and Nafion-Pt3Co/C interfaces in fuel cell. J Phys Chem C 116(40):21401–21406

42. Kunimatsu K, Yoda T, Tryk DA, Uchida H, Watanabe M (2010) In situ ATR-FTIR study of oxygen reduction at the Pt/Nafion interface. Phys Chem Chem Phys 12(3):621–629

43. Kendrick I, Kumari D, Yakaboski A, Dimakis N, Smotkin ES (2010) Elucidating the ionomer-electrified metal interface. J Am Chem Soc 132(49):17611–17616

44. Ayato Y, Kunimatsu K, Osawa M, Okada T (2006) Study of Pt electrode/Nafion ionomer interface in HClO4 by in situ surface-enhanced FTIR spectroscopy. J Electrochem Soc 153(2):A203–A209

45. Mohamed HF et al (2013) Possible presence of hydrophilic SO3H nanoclusters on the surface of dry ultrathin Nafion(R) films: a positron annihilation study. Phys Chem Chem Phys 15(5):1518–1525

46. Paul DK, Giorgi JB, Karan K (2013) Chemical and ionic conductivity degradation of ultra-thin ionomer

film by X-ray beam exposure. J Electrochem Soc 160(4):F464–F469

47. Albert JNL, Epps Iii TH (2010) Self-assembly of block copolymer thin films. Mater Today 13(6):24–33

48. Segalman RA (2005) Patterning with block copolymer thin films. Mater Sci Eng R 48(6):191–226

49. Fasolka MJ, Mayes AM (2001) BLOCK COPOLYMER THIN FILMS: physics and Applications1. Annu Rev Mater Res 31(1):323–355

50. Russell TP, Lambooy P, Kellogg GJ, Mayes AM (1995) Diblock copolymers under confinement. Physica B 213(0):22–25

51. Huang E et al (1998) Using surface active random copolymers to control the domain orientation in diblock copolymer thin films. Macromolecules 31(22):7641–7650

52. Mansky P, Russell TP, Hawker CJ, Pitsikalis M, Mays J (1997) Ordered Diblock copolymer films on random copolymer brushes. Macromolecules 30(22):6810–6813

53. Modestino MA et al (2013) Self-assembly and transport limitations in confined Nafion films. Macromolecules 46(3):867–873

54. Bertoncello P, Ciani I, Li F, Unwin PR (2006) Measurement of apparent diffusion coefficients within ultrathin Nafion Langmuir-Schaefer films: comparison of a novel scanning electrochemical microscopy approach with cyclic voltammetry. Langmuir 22(25):10380–10388

55. Dishari SK, Hickner MA (2013) Confinement and proton transfer in NAFION thin films. Macromolecules 46(2):413–421

56. Ohira A, Kuroda S, Mohamed HFM, Tavernier B (2013) Effect of interface on surface morphology and proton conduction of polymer electrolyte thin films. Phys Chem Chem Phys 15(27):11494–11500

57. Modestino MA, Kusoglu A, Hexemer A, Weber AZ, Segalman RA (2012) Controlling Nafion structure and properties via wetting interactions. Macromolecules 45(11):4681–4688

58. Noguchi H, Taneda K, Minowa H, Naohara H, Uosaki K (2010) Humidity-dependent structure of surface water on Perfluorosulfonated ionomer thin film studied by sum frequency generation spectroscopy. J Phys Chem C 114(9):3958–3961

59. Novitski D, Xie Z, Holdcroft S (2015) Time-dependent mass transport for O-2 reduction at the Pt | Perfluorosulfonic acid ionomer Interface. ECS Electrochem Lett 4(1):F9–F12

60. Tang J, Yuan W, Zhang J, Li H, Zhang Y (2013) Evidence for a crystallite-rich skin on perfluorosulfonate ionomer membranes. RSC Adv 3(23):8947–8952

61. He Q et al (2011) Correlating humidity-dependent ionically conductive surface area with transport phenomena in proton-exchange membranes. J Phys Chem B 115(40):11650–11657

62. Bass M, Berman A, Singh A, Konovalov O, Freger V (2011) Surface-induced micelle orientation in Nafion films. Macromolecules 44(8):2893–2899

63. Koestner R, Roiter Y, Kozhinova I, Minko S (2011) AFM imaging of adsorbed Nafion polymer on mica and Graphite at molecular level. Langmuir 27(16):10157–10166

64. Paul DK, Karan K (2014) Conductivity and wettability changes of ultrathin Nafion films subjected to thermal annealing and liquid water exposure. J Phys Chem C 118(4):1828–1835

65. Ogata Y, Kawaguchi D, Yamada NL, Tanaka K (2013) Multistep thickening of Nafion thin films in water. ACS Macro Lett 2(10):856–859

66. Abuin GC, Cecilia Fuertes M, Corti HR (2013) Substrate effect on the swelling and water sorption of Nafion nanomembranes. J Membr Sci 428(0):507–515

67. Paul DK, Karan K, Docoslis A, Giorgi JB, Pearce J (2013) Characteristics of self-assembled ultrathin Nafion films. Macromolecules 46(9):3461–3475

68. Davis EM, Stafford CM, Page KA (2014) Elucidating water transport mechanisms in Nafion thin films. ACS Macro Lett 3(10):1029–1035

69. Shim HK, Paul DK, Karan K (2015) Resolving the contradiction between anomalously high water uptake and low conductivity of nanothin Nafion films on SiO2 substrate. Macromolecules 48(22):8394–8397

70. Paul DK, Shim HK, Giorgi JB, Karan K (2016) Thickness dependence of thermally induced changes in surface and bulk properties of Nafion (R) nanofilms. J Polym Sci Part B Polym Phys 54(13):1267–1277

71. Bertoncello P, Wilson NR, Unwin PR (2007) One-step formation of ultra-thin chemically functionalized redox-active Langmuir-Schaefer Nafion films. Soft Matter 3(10):1300–1307

72. Krtil P, Trojanek A, Samec Z (2001) Kinetics of water sorption in Nafion thin films – quartz crystal microbalance study. J Phys Chem B 105(33):7979–7983

73. Nadermann NK, Davis EM, Page KA, Stafford CM, Chan EP (2015) Using indentation to quantify transport properties of nanophase-segregated polymer thin films. Adv Mater 27(33) 4924–4930.

74. Springer TE, Zawodzinski TA, Gottesfeld S (1991) Polymer Electrolyte Fuel-Cell Model. J Electrochem Soc 138(8):2334–2342

75. Kusoglu A, Weber AZ (2017) New insights into perfluorinated sulfonic-acid ionomers. Chem Rev 117(3):987–1104

76. Pantelić N, Wansapura CM, Heineman WR, Seliskar CJ (2005) Dynamic in situ spectroscopic ellipsometry of the reaction of aqueous iron(II) with 2,2′-bipyridine in a thin Nafion film. J Phys Chem B 109(29):13971–13979

77. Bai YJ, Schaberg MS, Hamrock SJ, Tang ZJ, Goenaga G, Papandrew AB and Zawodzinski TA (2017) Density Measurements and Partial Molar Volume Analysis of Different Membranes for Polymer Electrolyte Membrane Fuel Cells. Electrochim Acta 242:307–314

78. Freger V (2009) Hydration of ionomers and Schroeder's paradox in Nafion. J Phys Chem B 113(1):24–36

79. Kreuer KD (2013) The role of internal pressure for the hydration and transport properties of ionomers and polyelectrolytes. Solid State Ionics 252(0):93–101

80. Kusoglu A, Savagatrup S, Clark KT, Weber AZ (2012) Role of mechanical factors in controlling the structure–function relationship of PFSA ionomers. Macromolecules 45(18):7467–7476

81. Kollath VO, Karan K (2016) New molecular scale insights into the alpha-transition of Nafion (R) thin films from variable temperature ATR-FTIR spectroscopy. Phys Chem Chem Phys 18(37):26144–26150

82. Singhal N, Datta A (2016) Thickness dependence of acidity and microstructure in Nafion films. Chemistryselect 1(10):2277–2283

83. Allen FI et al (2015) Morphology of hydrated as-cast Nafion revealed through Cryo electron tomography. ACS Macro Lett 4(1):1–5

84. Umemura K et al (2006) Nanocharacterization and nanofabrication of a Nafion thin film in liquids by atomic force microscopy. Langmuir 22(7):3306–3312

85. Hill TA, Carroll DL, Czerw R, Martin CW, Perahia D (2003) Atomic force microscopy studies on the dewetting of perfluorinated ionomer thin films. J Polym Sci Part B Polym Phys 41(2):149–158

86. Maeda Y et al (2008) Study of the nanoscopic deformation of an annealed Nafion film by using atomic force microscopy and a patterned substrate. Ultramicroscopy 108(6):529–535

87. De Almeida NE, Paul DK, Karan K, Goward GR (2015) 1H solid-state NMR study of Nanothin Nafion films. J Phys Chem C 119(3):1280–1285

88. Kalisvaart WP, Fritzsche H, Merida W (2015) Water uptake and swelling hysteresis in a Nafion thin film measured with neutron reflectometry. Langmuir 31(19):5416–5422

89. DeCaluwe SC, Kienzle PA, Bhargava P, Baker AM, Dura JA (2014) Phase segregation of sulfonate groups in Nafion interface lamellae, quantified via neutron reflectometry fitting techniques for multi-layered structures. Soft Matter 10(31):5763–5776

90. Hexemer A, Müller-Buschbaum P (2015) Advanced grazing-incidence techniques for modern soft-matter materials analysis. IUCrJ 2(Pt 1):106–125

91. Nagao Y (2017) Proton-conductivity enhancement in polymer thin films. Langmuir 33(44):12547–12558

92. Peron J et al (2011) Fuel cell catalyst layers containing short-side-chain perfluorosulfonic acid ionomers. J Power Sources 196(1):179–181

93. Dorenbos G, Pomogaev VA, Takigawa M, Morohoshi K (2010) Prediction of anisotropic transport in Nafion containing catalyst layers. Electrochem Commun 12(1):125–128

94. Hwang GS, Parkinson DY, Kusoglu A, MacDowell AA, Weber AZ (2013) Understanding water uptake and transport in Nafion using X-ray microtomography. ACS Macro Lett 2(4):288–291

95. Novitski D, Holdcroft S (2015) Determination of O-2 mass transport at the Pt I PFSA ionomer interface under reduced relative humidity. ACS Appl Mater Interfaces 7(49):27314–27323

96. Uribe FA, Springer TE, Gottesfeld S (1992) A microelectrode study of oxygen reduction at the platinum/recast-Nafion film Interface. J Electrochem Soc 139(3):765–773

97. Sambandam S, Parrondo J, Ramani V (2013) Estimation of electrode ionomer oxygen permeability and ionomer-phase oxygen transport resistance in polymer electrolyte fuel cells. Phys Chem Chem Phys: PCCP 15(36):14994–15002

98. Zhang L, Ma CS, Mukerjee S (2004) Oxygen reduction and transport characteristics at a platinum and alternative proton conducting membrane interface. J Electroanal Chem 568(1–2):273–291

99. Nouri-Khorasani A et al (2016) Molecular modeling of the proton density distribution in a water-filled slab-like nanopore bounded by Pt oxide and ionomer. Catal Today 262:133–140

100. Garrick TR, Moylan TE, Yarlagadda V, Kongkanand A (2017) Characterizing electrolyte and platinum Interface in PEM fuel cells using CO displacement. J Electrochem Soc 164(2):F60–F64

101. Subbaraman R, Strmcnik D, Stamenkovic V, Markovic NM (2010) Three phase interfaces at electrified metal-solid electrolyte systems 1. Study of the Pt(hkl)-Nafion Interface. J Phys Chem C 114(18):8414–8422

102. Andersen SM et al (2014) Adsorption behavior of perfluorinated sulfonic acid ionomer on highly graphitized carbon nanofibers and their thermal stabilities. J Phys Chem C 118(20):10814–10823

103. Masuda T, Naohara H, Takakusagi S, Singh PR, Uosaki K (2009) Formation and structure of perfluorosulfonated ionomer thin film on a graphite surface. Chem Lett 38(9):884–885

104. Damasceno Borges D, Gebel G, Franco AA, Malek K, Mossa S (2015) Morphology of supported polymer electrolyte ultrathin films: a numerical study. J Phys Chem C 119(2):1201–1209

105. Mashio T et al (2010) Molecular dynamics study of ionomer and water adsorption at carbon support materials. J Phys Chem C 114(32):13739–13745

106. Jinnouchi R, Kudo K, Kitano N, Morimoto Y (2016) Molecular dynamics simulations on O-2 permeation through Nafion ionomer on platinum surface. Electrochim Acta 188:767–776

107. Kanamura K, Morikawa H, Umegaki T (2003) Observation of interface between Pt electrode and Nafion membrane. J Electrochem Soc 150(2):A193–A198

108. He QP, Suraweera NS, Joy DC, Keffer DJ (2013) Structure of the ionomer film in catalyst layers of proton exchange membrane fuel cells. J Phys Chem C 117(48):25305–25316

109. Kodama K et al (2013) Increase in adsorptivity of sulfonate anions on Pt (111) surface with drying of ionomer. Electrochem Commun 36:26–28